Supplementary of Seasonal to long-term variability of natural and anthropogenic carbon concentrations and transports in the subpolar North Atlantic Ocean

Raphaël Bajon [1], Lidia I. Carracedo [1], Herlé Mercier [1], Rémy Asselot [2], and Fiz F. Pérez [3]

[1]Laboratoire d'Océanographie Physique et Spatiale (UMR 6523 LOPS), Univ. Brest, CNRS, IFREMER, IRD, IUEM, IFREMER Centre de Bretagne, 29280 Plouzané, FRANCE
[2]BRGM, 24 avenue Léonard de Vinci, F-33600 Pessac, France
[3]Oceanographic department, IIM, Street, Vigo, 10587, Pontevedra, SPAIN

Correspondence: Raphaël Bajon (raphael.bajon@ifremer.fr)

Most of the supplementary materials focus on adding information on the method used in this study to derive $[C_{nat}]$ and $[C_{ant}]$ from T, S of the ocean reanalysis. Detailed tables with RMSD obtained using the NN method on the hydrographic data of A25 are provided (Tables S1–S5). Additional comparisons between A25 observations and ocean reanalysis are added for volume, C_{nat} and C_{ant} transports (Tables S6 –S8). Supplementary figures provided information on the seasonal and interannual signal of $[C_{nat}]$ and $[C_{ant}]$, as well as layer average and surface concentrations. The evolution of uMOC and ML depth is also presented, along with specific results from the GLOSEA5 reanalysis and the OR-NN-BC method.

Supplementary Text S1: DIC data uncertainty

The uncertainty in DIC is coming from the bottle measurement of pH_T and alkalinity. In terms of precision, considering that the pH_T accuracy is 0.0055 (Carter et al., 2013) and the alkalinity accuracy is 2 μmol kg^{-1} (Blasco and Tovar-Sánchez, 2023), this implies an uncertainty of 5.8 μmol kg^{-1}, also considering the uncertainties in the thermodynamic constants of the marine carbonate system (Orr et al., 2018).

Supplementary Tables

Tab. S1. RMSD at A25 between [O_2], [DIC] and [C_{ant}] computed with the NN-method (2.9.1) and the estimations derived from sea bottle measurements (2.3). The units are μmol kg^{-1} for the three variables. (**) In the two right columns, O_2 is not calculated and [DIC] and [C_{ant}] are calculated using T, S and O_2 from bottle samples (2.3). (*) For the three columns with T and S from bottles as inputs, O_2 is calculated with ESPER NN equation 8 Carter et al. (2021) (see the methods in 2.8). CANYON-B-CONTENT Bittig et al. (2018) is run to obtain DIC according to our method, and the macronutrients needed to obtain C_{ant} come from ESPER calculations.

Input Bottle Variable	T, S (*)			T, S, O_2 (**)	
A25 year	O_2	DIC	C_{ant}	DIC	C_{ant}
2002	7.2	6.6	3.6	4.1	3.1
2004	8.1	14.7	6.4	15.1	6.5
2006	8.0	8.0	4.8	8.3	4.1
2008	6.7	8.8	5.0	9.3	4.8
2010	6.8	8.7	5.2	8.4	4.8
2012	9.4	9.2	3.5	7.4	2.5
2014	9.5	6.7	3.3	4.7	2.2
2016	7.3	14.6	8.0	14.3	7.7
2018	7.2	7.3	4.4	7.4	3.7
2002–2018 (SE)	7.8 (0.3)	9.7 (1.0)	5.1 (0.5)	9.5 (1.3)	4.7 (0.6)

Tab. S2. Table 3 details: RMSD (for each layer) of [C_{nat}] and [C_{ant}] computed with the NN-method averaged over the ocean reanalysis compared to the estimations derived from sea bottle measurements at the A25 cruise (2002-2018). The units are μmol kg^{-1}. The comparison is made in June for each A25 year.

A25 year	C_{nat}			C_{ant}		
	net	uMOC	lMOC	net	uMOC	lMOC
2002	1.5	0.6	2.2	2.0	1.5	1.0
2004	2.7	2.0	2.6	1.6	1.8	0.4
2006	0.5	0.6	0.1	1.3	1.1	0.3
2008	1.2	0.5	1.4	0.6	0.4	0.6
2010	1.0	1.5	1.5	0.6	1.3	0.7
2012	0.2	0.1	0.5	1.2	0.8	0.2
2014	0.7	0.4	2.6	1.5	0.1	1.1
2016	1.2	5.0	0.2	0.1	1.7	1.0
2018	1.7	4.3	3.0	0.4	0.5	0.2
2002–2018	1.4	2.4	1.9	1.2	1.2	0.7

Tab. S3. Table 4 details: RMSD of [C_{nat}] and [C_{ant}] for the uMOC (resolved with each ocean reanalysis) computed with the NN-method over the ocean reanalysis compared to the estimations derived from sea bottle measurements at the A25 cruise (2002-2018). The units are μmol kg^{-1}. The comparison is made in June for each A25 year. The difference is solely due to the differences between the T, S of the reanalyses and the observed T, S.

A25 year	uMOC C_{nat}				
	GLOSEA5	ECCO	EN4	CORA	GOBAI-O$_2$
2002	2.9	3.9	0.8	1.3	x
2004	0.3	9.1	1.7	1.4	0.7
2006	2.0	0.2	2.0	1.4	1.8
2008	1.2	6.0	0.2	4.6	3.7
2010	2.1	4.9	1.1	1.2	2.4
2012	0.5	5.5	7.2	0.7	0.3
2014	2.1	4.7	3.4	1.4	0.9
2016	6.5	1.7	7.1	7.8	5.2
2018	3.3	x	9.9	7.6	5.9
2002–2018	2.9	5.2	4.9	4.1	3.3

A25 year	uMOC C_{ant}				
	GLOSEA5	ECCO	EN4	CORA	GOBAI-O$_2$
2002	1.5	0.3	2.8	3.0	x
2004	1.8	1.6	1.5	2.5	2.0
2006	0.9	0.9	2.9	1.6	1.3
2008	0.7	0.4	1.4	0.8	0.1
2010	0.2	0.5	1.1	1.8	2.2
2012	1.3	0.4	1.5	1.1	1.7
2014	1.4	0.6	1.2	0.5	0.6
2016	2.3	3.1	1.6	2.3	0.9
2018	2.1	x	2.9	1.9	1.0
2002–2018	1.5	1.3	2.0	1.9	1.4

Tab. S4. Table 4 details: RMSD (for each layer) of the integrated transport variables ($T_{C_{nat}}$, $T_{C_{ant}}$: transport of C_{nat}, C_{ant} respectively) with property computed with the NN-method averaged over the ocean reanalysis compared to the estimations derived from sea bottle measurements at the A25 cruise (2002-2018). The units are PgC yr^{-1}. The comparison is made in June for each A25 year. We add a decimal place for $T_{C_{ant}}$ because its amplitude is an order of magnitude smaller than that of $T_{C_{nat}}$.

A25 year	$T_{C_{nat}}$			$T_{C_{ant}}$		
	net	uMOC	lMOC	net	uMOC	lMOC
2002	0.8	0.8	0.7	0.01	0.03	0.02
2004	0.04	0.3	1.2	0.01	0.01	0.03
2006	0.7	3.0	5.3	0.04	0.09	0.10
2008	0.9	3.5	0.6	0.02	0.07	0.02
2010	1.5	1.5	0.9	0.04	0.02	0.04
2012	0.6	1.6	0.2	0.01	0.05	0.01
2014	0.7	0.1	1.1	0.05	0.01	0.04
2016	0.5	0.6	1.4	0.04	0.001	0.07
2018	0.2	0.6	5.0	0.09	0.04	0.06
2002–2018	0.8	1.7	2.6	0.04	0.05	0.05

Tab. S5. Table 4 details: RMSD of the integrated transport variables ($T_{C_{nat}}$, $T_{C_{ant}}$: transport of C_{nat}, C_{ant} respectively) for the upper branch of the Atlantic Meridional Overturning Circulation (resolved with each ocean reanalysis) with property computed with the NN-method over the ocean reanalysis compared to the estimations derived from sea bottle measurements at the A25 cruise (2002–2018). The units are PgC yr^{-1}. The comparison is made in June for each A25 year. We add a decimal place for $T_{C_{ant}}$ because its amplitude is an order of magnitude smaller than that of $T_{C_{nat}}$.

| A25 year | uMOC $T_{C_{nat}}$ | | | | |
	GLOSEA5	ECCO	EN4	CORA	GOBAI-O$_2$
2002	1.4	0.9	2.6	0.2	x
2004	3.7	1.4	0.04	1.4	1.2
2006	6.7	2.4	2.8	2.1	2.1
2008	2.1	2.5	4.3	6.5	4.0
2010	2.2	3.2	1.7	1.9	2.4
2012	1.9	3.2	3.1	1.9	3.8
2014	3.9	3.0	0.2	0.1	0.3
2016	2.0	3.7	1.7	1.4	1.1
2018	5.3	x	0.5	0.8	1.2
2002–2018	3.7	2.7	2.3	2.6	2.4

| A25 year | uMOC $T_{C_{ant}}$ | | | | |
	GLOSEA5	ECCO	EN4	CORA	GOBAI-O$_2$
2002	0.05	0.00	0.05	0.02	x
2004	0.09	0.01	0.01	0.01	0.02
2006	0.17	0.09	0.09	0.08	0.07
2008	0.05	0.05	0.08	0.13	0.07
2010	0.07	0.05	0.03	0.03	0.03
2012	0.07	0.05	0.06	0.07	0.12
2014	0.06	0.08	0.04	0.01	0.00
2016	0.03	0.1	0.01	0.02	0.02
2018	0.15	x	0.01	0.01	0.01
2002–2018	0.09	0.06	0.05	0.06	0.06

Tab. S6. Volume transport of the ocean reanalysis: mean value, STD and RMSD to A25 for the different water layers

Layer	Ocean product	Mean ($\pm 2\varepsilon$)	STD	RMSD A25
uMOC	CORA	18.8±0.83	4.3	3.1
	EN4	20.7±0.87	4.3	2.8
	GLOSEA5	19.6±0.55	2.7	4.3
	ECCO	15.1±0.85	2.5	3.2
lMOC	GLOSEA5	-18.7±0.51	2.8	4.5
	ECCO	-14.9±0.54	2.6	3.0
net	GLOSEA5	0.85±0.65	1.1	0.8
	ECCO	0.2±0.1	0.7	1.1

Tab. S7. C_{nat} transport of the ocean products: mean value, STD and RMSD to A25 for the different water layers

Layer	Ocean product	Mean ($\pm 2\varepsilon$)	STD	RMSD A25
uMOC	CORA	15.3±0.68	3.6	2.6
	EN4	16.9±0.72	3.7	2.3
	GLOSEA5	16.2±0.46	2.3	3.7
	ECCO	12.4±0.7	2.0	2.7
	GOBAI-O_2	14.6±0.70	3.0	2.4
lMOC	GLOSEA5	-15.5±0.43	2.3	3.8
	ECCO	-12.3±0.46	2.1	2.4
net	GLOSEA5	0.62±0.53	0.91	0.7
	ECCO	0.04±0.09	0.6	1.0

Tab. S8. C_{ant} transport of the ocean products: mean value, STD and RMSD to A25 for the different water layers

Layer	Ocean product	Mean ($\pm 2\varepsilon$)	STD	RMSD A25
uMOC	CORA	0.35±0.02	0.08	0.057
	EN4	0.37±0.04	0.09	0.050
	GLOSEA5	0.37±0.04	0.06	0.094
	ECCO	0.28±0.01	0.05	0.064
	GOBAI-O_2	0.35±0.02	0.08	0.059
lMOC	GLOSEA5	-0.27±0.02	0.04	0.069
	ECCO	-0.19±0.01	0.04	0.056
net	GLOSEA5	0.10±0.02	0.03	0.043
	ECCO	0.09±0.01	0.02	0.032
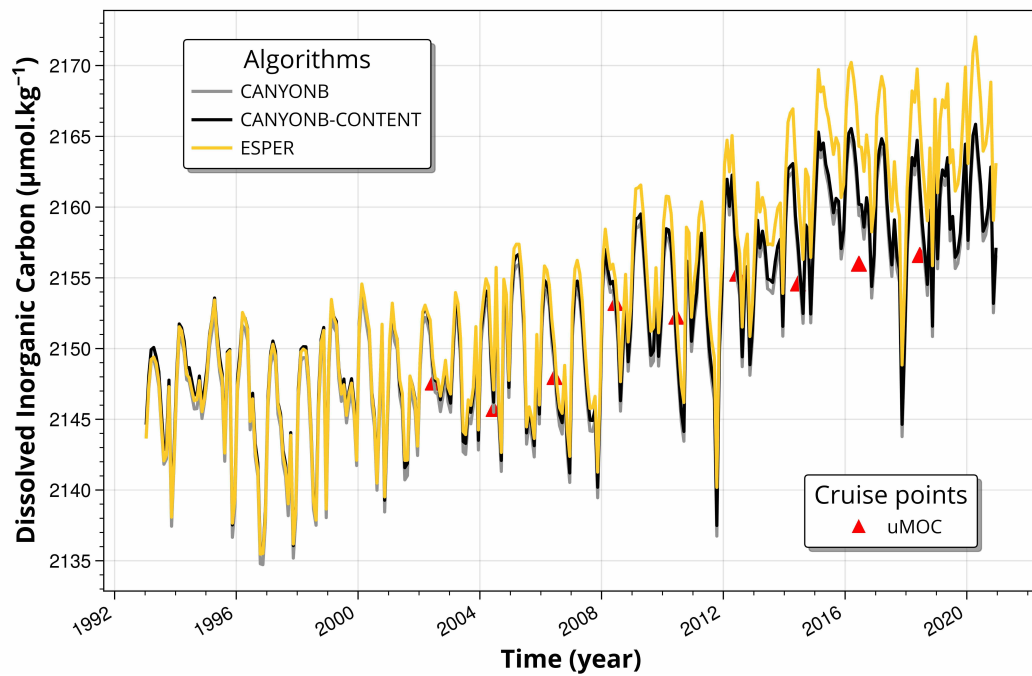
Fig. S1. DIC calculated by different NN methods (ESPER (Carter et al., 2021), CANYON-B and CANYON-B-CONTENT (Bittig et al., 2018)) using the CORA reanalysis fields as input variables and averaged for the uMOC. CANYON-B-CONTENT is chosen for the results section.

Average depth for ML and uMOC (m)

Fig. S2. Left panels) time series of ML Depth (in m) and uMOC thickness for the different ocean reanalyses. The dashed red lines represent the interannual signal. Right panels) Seasonality is computed applying a two-year high pass filter as described in Methods and shown here as anomaly.
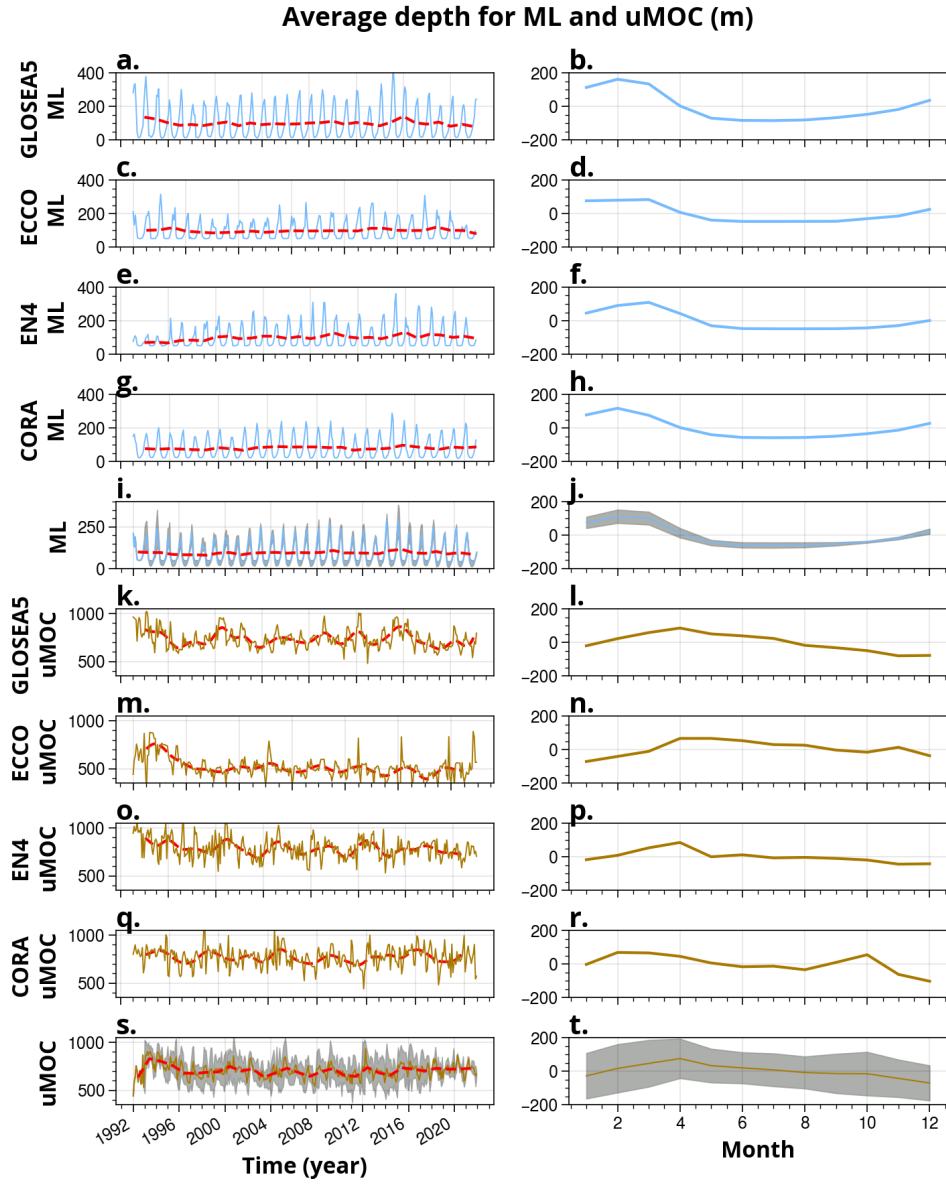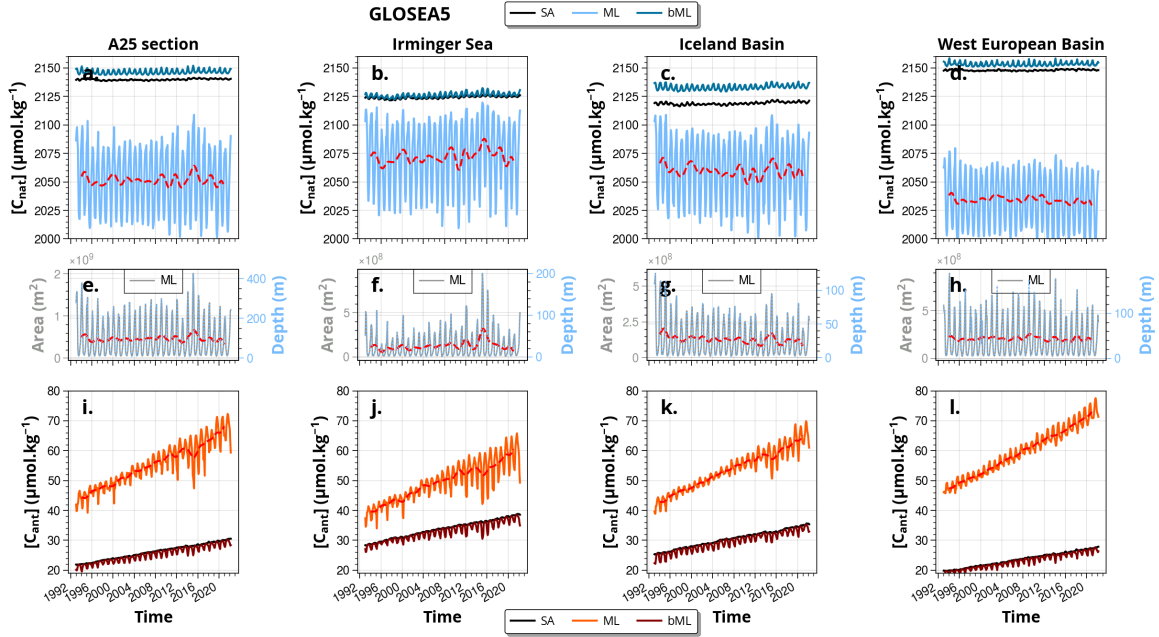
Fig. S3. Natural carbon concentration [C_{nat}] (top panels), variation of the ML area/depth (middle panels) and anthropogenic carbon concentration [C_{ant}] (bottom panels), for GLOSEA5. The dashed red line represents the interannual signal for the ML. The full A25 section is separated into the Irminger Sea (West of the Reykjanes Ridge, longitudes inferior to -31°E), the Iceland basin (longitudes between -31°E and -24.5°E) and the West European Basin (longitudes superior to -24.5°E) (Fig. 1). SA refers to section averaged.
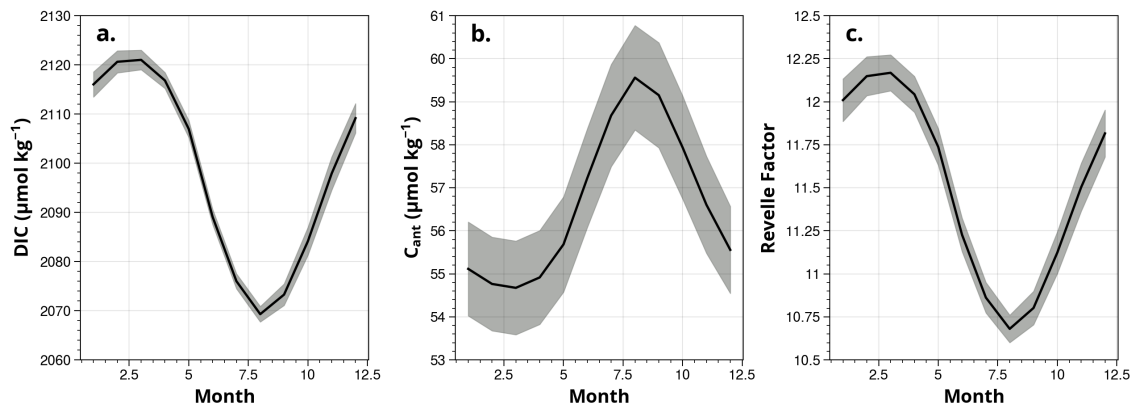
Fig. S4. (a) DIC, (b) [C_{ant}] and (c) Revelle Factor at 5m depth, obtained from OR-NN-BC and averaged between reanalyses. The standard errors (STDns) are shown in grey shading.
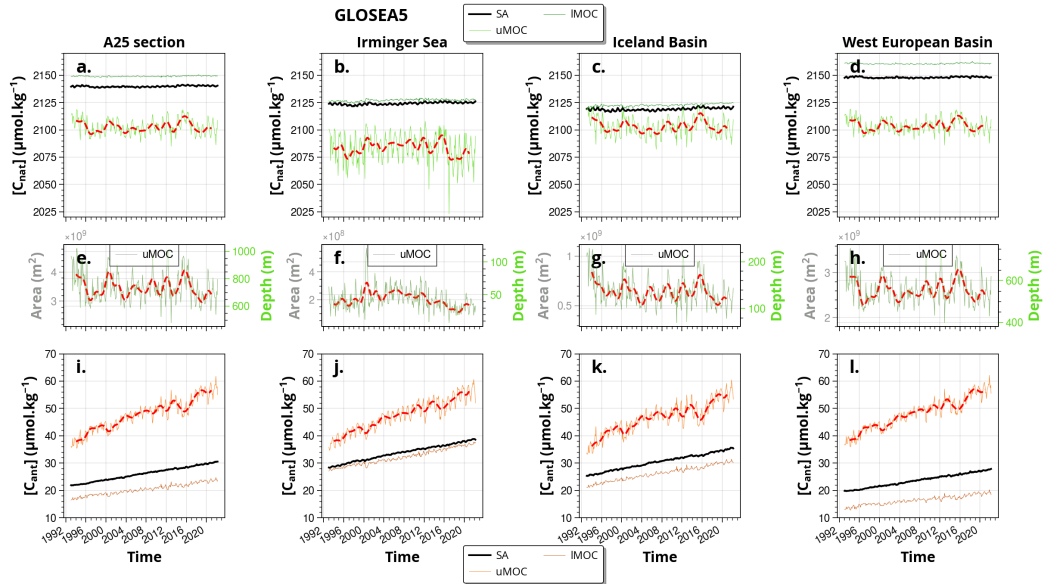
Fig. S5. Natural carbon concentration [C_{nat}] (top panels), variation of the MOC area/depth (middle panels) and anthropogenic carbon concentration [C_{ant}] (bottom panels), for GLOSEA5. The dashed red line represents the interannual signal for the ML. The full A25 section is separated into the Irminger Sea (West of the Reykjanes Ridge, longitudes inferior to -31°E), the Iceland basin (longitudes between -31°E and -24.5°E) and the West European Basin (longitudes superior to -24.5°E) (Fig. 1). SA refers to section averaged.
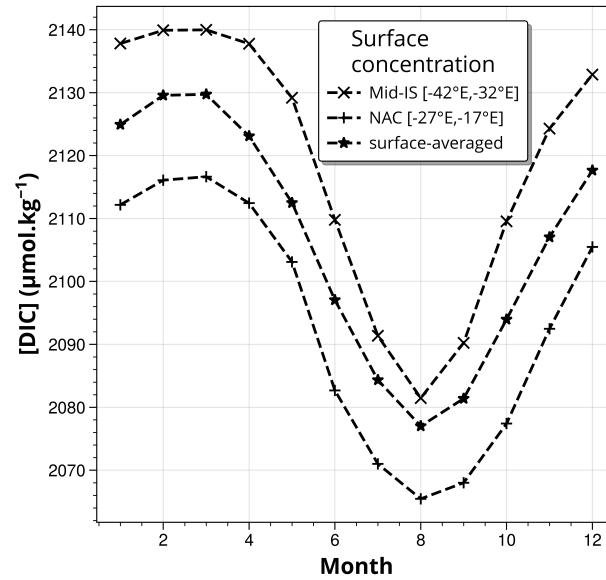
Fig. S6. Seasonal cycle of surface [DIC] concentration for the middle of the Irminger Sea (between -42°E and -32°E, cross symbols), the NAC (between -27°E and -17°E, plus symbols) and the full-section average (star symbols). Here, seasonal cycles are obtained by grouping the time series signal of [DIC] by month and averaging. The time series are subsets of the complete series of Fig. 2, sampled from 2004 to 2017, in order to have all reanalyses defined in the period (Table 1). Values represent the average of all ocean reanalyses.
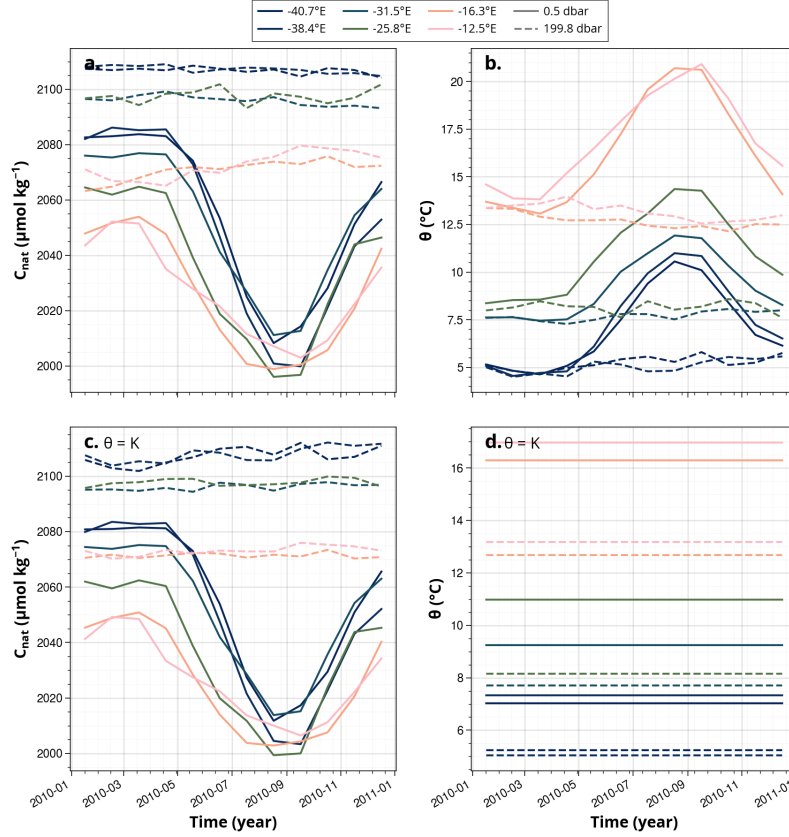
Fig. S7. (a) [C$_{nat}$] predictions using seasonal potential temperature displayed in (b) and (c) [C$_{nat}$] predictions using a fixed value K for each longitude and depth displayed in (d), for GLOSEA5 and the example seasonal cycle of 2010. All the other inputs of the φC$_T^0$ approach (i.e. year, position, salinity, oxygen, nitrate, phosphate, silicate, alkalinity, dissolved inorganic carbon) are the same between (a) and (c). The continuous lines correspond to 0.5 dbar while the dashed lines to 199.8 dbar. The colors (blue to pink) are referring to the different positions along the A25 section: -40.7°E, -38.4°E, -31.5°, -25.8°, -16.3°E, -12.5°E.
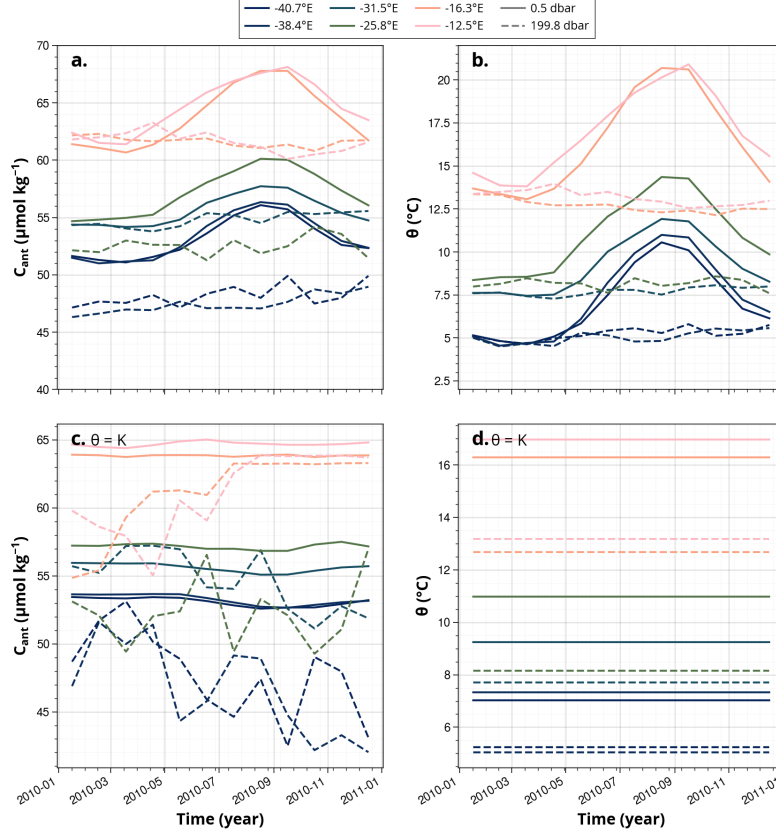
Fig. S8. (a) $[C_{ant}]$ predictions using seasonal potential temperature displayed in (b) and (c) $[C_{ant}]$ predictions using a fixed value K for each longitude and depth displayed in (d), for GLOSEA5 seasonal cycle of 2010. All the other inputs of the φC_T^0 approach (i.e. year, position, salinity, oxygen, nitrate, phosphate, silicate, alkalinity, dissolved inorganic carbon) are the same between (a) and (c). The continuous lines correspond to 0.5 dbar while the dashed lines to 199.8 dbar. The colors (blue to pink) are referring to the different positions along the A25 section: -40.7°E, -38.4°E, -31.5°, -25.8°, -16.3°E, -12.5°E.
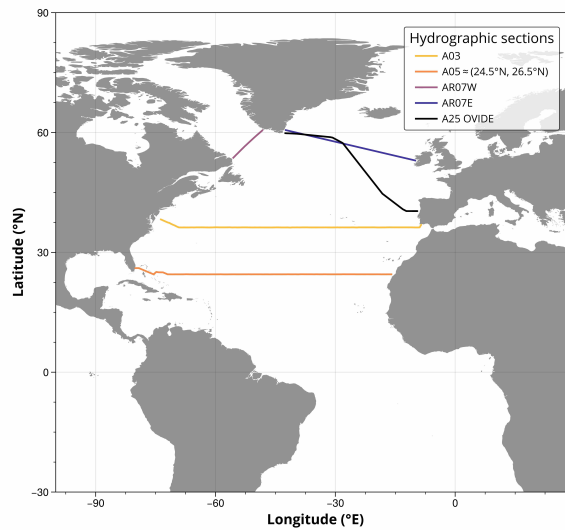
Fig. S9. Map of the zonal sections cited. Please note that the position of the sections may vary slightly depending on the year of measurement. The position of sections 24.5°N and 26.5°N is similar to A05.

References

15 Bittig, H. C., Steinhoff, T., Claustre, H., Fiedler, B., Williams, N. L., Sauzède, R., Körtzinger, A., and Gattuso, J.-P.: An Alternative to Static Climatologies: Robust Estimation of Open Ocean CO2 Variables and Nutrient Concentrations From T, S, and O2 Data Using Bayesian Neural Networks, Frontiers in Marine Science, 5, 328, https://doi.org/10.3389/fmars.2018.00328, 2018.

Blasco, J. and Tovar-Sánchez, A., eds.: Marine Analytical Chemistry, Springer eBook Collection, Springer International Publishing, Cham, 1st ed. 2023 edn., ISBN 978-3-031-14486-8, https://doi.org/10.1007/978-3-031-14486-8, 2023.

20 Carter, B. R., Bittig, H. C., Fassbender, A. J., Sharp, J. D., Takeshita, Y., Xu, Y., Álvarez, M., Wanninkhof, R., Feely, R. A., and Barbero, L.: New and updated global empirical seawater property estimation routines, Limnology and Oceanography: Methods, 19, 785–809, https://doi.org/10.1002/lom3.10461, 2021.

Carter, H. A., Ceballos-Osuna, L., Miller, N. A., and Stillman, J. H.: Impact of ocean acidification on metabolism and energetics during early life stages of the intertidal porcelain crab *Petrolisthes cinctipes*, Journal of Experimental Biology, 216, 1412–1422,

25 https://doi.org/10.1242/jeb.078162, publisher: The Company of Biologists, 2013.

Orr, J. C., Epitalon, J.-M., Dickson, A. G., and Gattuso, J.-P.: Routine uncertainty propagation for the marine carbon dioxide system, Marine Chemistry, 207, 84–107, https://doi.org/10.1016/j.marchem.2018.10.006, publisher: Elsevier BV, 2018.